Chitosan/collagen biomembrane loaded with 2,3-dihydrobenzofuran for the treatment of cutaneous Leishmaniasis

Elton Marks Araujo Braz[a], *Solranny Carla Cavalcante Costa Silva*[a,b], *Michel Muálem Moraes Alves*[c,d], *Fernando Aécio Amorim Carvalho*[c,*], *Rui Magalhães*[e], *Josy Anteveli Osajima*[a], *Durcilene Alves Silva*[a,*], *Ana Leite Oliveira*[e,*], *Edvani Curti Muniz*[a,f], *Edson Cavalcanti Silva-Filho*[a,*,#]

[a] Laboratório Interdisciplinar de Materiais Avançados – LIMAV, Universidade Federal do Piauí, Campus Ministro Petrônio Portella, Teresina, PI - 64049-550, Brazil.

[b] Universidade Estadual do Piauí, Campus Professor Ariston Dias Lima, São Raimundo Nonato, PI - 64770-000, Brazil.

[c] Núcleo de Pesquisa em Plantas Medicinais – NPPM, Universidade Federal do Piauí, Campus Ministro Petrônio Portella, Teresina, PI - 64049-550, Brazil.

[d] Departamento de Morfofisiologia Veterinária, Universidade Federal do Piauí, Campus Ministro Petrônio Portella, Teresina, PI - 64049-550, Brazil.

[e] Universidade Católica Portuguesa, CBQF - Centro de Biotecnologia e Química Fina – Laboratório Associado, Escola Superior de Biotecnologia- Porto - 4169-005, Portugal.

[f] Universidade Estadual de Maringá, Departamento de Química, Maringá, PR – 87020-970, Brazil.

*Joint senior authors

[#] Correspondent author. E-mail: edsonfilho@ufpi.edu.br

GRAPHIC ABSTRACT

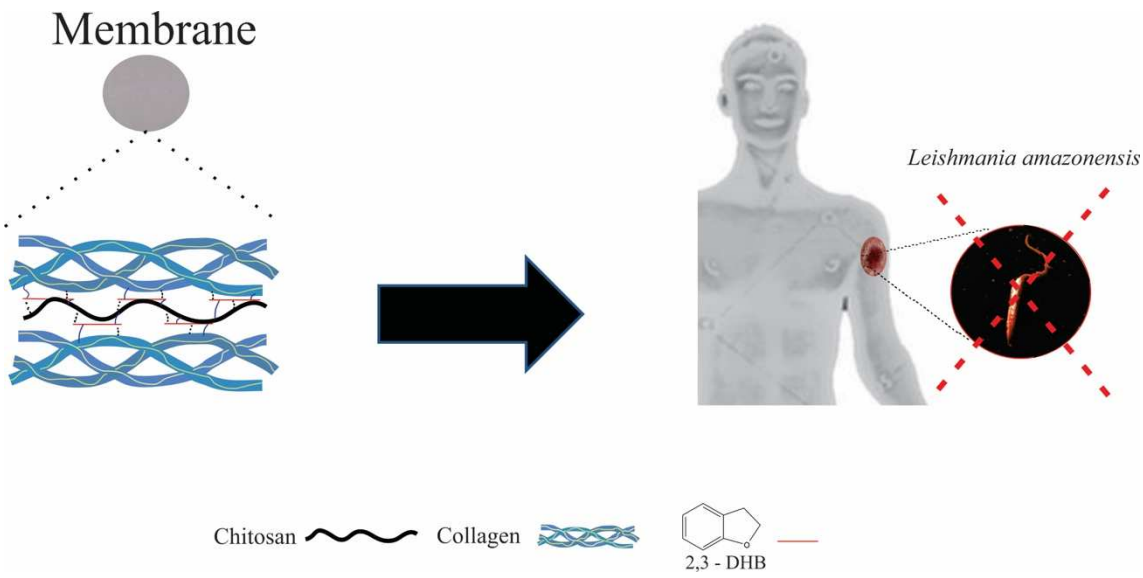

HIGHLIGHTS

- Biomembrane has potential for the treatment of cutaneous Leishmaniasis.
- The biomembrane stimulated the proliferation of human keratinocyte – HaCaT.
- AFM images showed excellent results in inhibiting parasite growth.

ABSTRACT

In this work, a chitosan/collagen-based membrane loaded with 2,3-dihydrobenzofuran (2,3-DHB) was developed through a simple solvent-casting procedure for use in the treatment of cutaneous Leishmaniasis. The obtained membranes were characterized by elemental analysis, FTIR, TG, DSC, and XRD. Porosity, swelling, mechanical properties, hydrophilicity, and antioxidant activity were analyzed. In addition, an assessment of the biocompatibility with fibroblasts and keratinocytes and of the *in vitro* wound healing was performed. The obtained results show that the new 2,3-DHB loaded chitosan/collagen membrane presented high porosity and swelling capacity as well as maximum strength, hydrophilicity, and antioxidant activity higher in relation to the control. The tests of antileishmanial activity and the AFM images great efficacy of inhibition growth of the parasite, superior to those of Amphotericin B, the standard therapeutic agent that is currently used. The new membranes are biocompatible and stimulated the proliferation of keratinocytes. SEM images clearly demonstrate that fibroblasts were able to adhere maintained their characteristic morphology. The healing test evidenced that the membranes have an adequate environment for promoting cell proliferation and growth. The new membrane proved to be an excellent candidate to treat cutaneous Leishmaniasis and is clearly indicated for further advanced studies *in vivo*.

Keywords: Polysaccharide; *Leishmania amazonensis*; wound treatment.

1. INTRODUCTION

Leishmaniasis are diseases caused by protozoa that belongs to the *Leishmania* genus. They are part of the neglected infectious diseases group with a wide global distribution since they affect the most vulnerable populations in the poorest countries [1]. The current pharmacological treatment of Leishmaniasis consists of limited therapies, which cause serious side effects, and the majority of the drugs used are only effective when administered parenterally, requiring long periods of therapy [2,3]. In addition, the parasites that cause Leishmaniasis have become resistant to drugs conventionally used in medical treatments [4,5], which makes the research of new antileishmanial compounds or alternative treatment therapies essential.

L. amazonensis causes cutaneous Leishmaniasis in humans and domestic animals [6,7], with a variety of symptoms, from self-healing infections to disfiguring chronic illnesses [8]. 2,3-dihydrobenzofuran (2,3-DHB) is a neolignan that recently has been studied for its potential as an antileishmania agent. It promoted high *in vitro* antileishmanial activity in the promastigote and amastigote forms of *Leishmania amazonensis*, with minimal cytotoxic effects in murine macrophages and human red blood cells. In addition, 2,3-DHB stimulated increased lysosomal volume, phagocytic capacity, and production of nitric oxide in macrophages, which are mechanisms possibly involved in its antileishmanial effect [9]. In this sense, 2,3-DHB could be used *in situ,* against the parasite that causes cutaneous Leishmaniasis, which produces wounds that are difficult to heal. Also, if incorporated as an active principle into a wound dressing, it could be useful to add leishmanicidal activity, while promoting wound healing.

Some biopolymers, such as collagen and chitosan, have already been widely used to treat wounds due to their intrinsic properties. Collagen is a fibrous protein that contributes to physiological functions of tissues in skin, tendons, bones, and cartilage

[10]. Furthermore, collagen has characteristics of biocompatibility, degradation, low antigenicity and plays an important role in tissue healing [11–13] since it provides the biological microenvironment for cell growth, supporting cell binding, migration, and proliferation [14,15]. Many collagen-related products have been developed in the recent years for wound healing, which demonstrates well its value as a biopolymer in regenerative medicine [16,17]. Chitosan is another well-known material for several applications [18,19], and its biocompatibility, biodegradability, non-toxicity, mucoadhesion, antimicrobial activity have been widely studied. This low cost and abundant polysaccharide [20–23] can promote wound healing, improving the functions of fibroblasts, macrophages and inflammatory cells [24], while exhibiting excellent film/membrane forming properties and water absorption capacity [25–27].

In addition, the combination of chitosan and collagen properties leads to improved materials that can be used to improve the healing of skin wounds [15,28], without causing inflammatory reaction [29], while simultaneously acting as a vehicle to release drugs such as dexamethasone [30] and gentamicin [31] due to their inherent properties. Consequently, anti-inflammatory drugs, pro-proliferative drugs and pre-synthesized membranes can be combined and employed to accelerate wound healing. Thus, a chitosan/collagen membrane with associated 2,3-DHB could be an excellent option for the treatment of cutaneous Leishmaniasis. Therefore, the objective of this work was to develop, for the first time, a membrane based on chitosan, collagen, and 2,3-DHB to treat wounds caused by *Leishmania.*

2. EXPERIMENTAL PART

2.1 Materials and reagents

115 Chitosan with medium degree of deacetylation 78% was obtained from Polymar.
116 Hydrolyzed collagen of bovine origin was obtained from Relva Verde Alimentos Ltda.
117 (Paraná, Brazil). To test antileishmanial activity, the promastigote forms of *L.*
118 *amazonensis* (IFLA/BR/67/PH8) were provided by the Antileishmanial Activity
119 Laboratory at the Federal University of Piauí. The antibiotic
120 (penicillin/streptomycin/amphotericin B) and trypsin were supplied by Lonza, USA. The
121 reagents 2,3-dihydrobenzofuran (2,3-DHB), acetic acid, absolute ethanol, potassium
122 persulfate, methanol, glutaraldehyde, dimethylsulfoxide (DMSO), MTT (3- [4,5-
123 dimethylthiazol-zyl]-2,5-diphenyltetrazolium bromide), phosphate-saline buffer (PBS),
124 Schneider's medium, resazurin, ABTS [2,2-azino-bis (3-ethylbenzothiazoline-6-
125 sulphonic acid)] and trolox were from Sigma-Aldrich. The human keratinocyte cell line
126 (HaCaT) was obtained from Cell Line Services (Oppenheim, Denmark) and were
127 cultured, as well as, the mouse fibroblast cells, L929 (NCTC) (ECACC 85103115), at
128 37 °C in a humidified atmosphere of 95% air and 5% CO_2, as monolayers using
129 Dulbecco's Modified Eagle's Medium (DMEM) with 4.5 $g.L^{-1}$ glucose, L-glutamine
130 without pyruvate (Lonza, Verviers, Belgium) containing 10% (v/v) fetal bovine serum
131 (FBS, Biowest, Nuaillé, France) and 1% (v/v) Penicillin-Streptomycin-Fungizone
132 (Lonza, Verviers, Belgium). The water used for the synthesis processes was obtained by
133 purification in a Milli-Q system (Millipore Corporation). All reagents were used without
134 prior purification.

135 **2.2 Membranes' production**

136 A 2.0% w/v chitosan solution was prepared in 0.1 $mol.L^{-1}$ of acetic acid. After
137 stirring overnight, the solution was rested to remove bubbles. A 2.0% w/v collagen
138 solution was prepared in the same way. The two solutions were mixed in a 1:1 ratio and
139 this mixture was stirred for 3 h using a magnetic stirrer. The membranes were prepared

by solvent casting technique in 96-well plates (100.0 µL of the solution per well) and 24-well plates (1000.0 µL of the solution per well) and dried in an oven for 48 h at 40 °C and called MQC.

A different batch of samples was produced by adding 2,3-dihydrobenzofuran (2,3-DHB) to the initial chitosan/collagen solution, to obtain a final concentration of 13.0 $\mu mol.L^{-1}$. This solution was stirred for 3 h and the membranes were prepared by solvent casting according to the previously described procedure. These were designated MDHB.

2.3 Characterization

Thermogravimetric analysis (TG, DTG, and DSC) was performed on the TA Instruments SDT Q600 V20.9 Build 20 device using approximately 10.0 mg of sample with a heating rate of 10 °C min^{-1} in an Argon atmosphere with a flow of 100.0 $mL.min^{-1}$ in an alumina sample holder in the temperature range from 25 to 800 °C. FTIR spectra of the materials were obtained using the Varian 660-IR spectrophotometer in 32 scans in the region of 500 to 4000 cm^{-1} with a resolution of 4 cm^{-1}. Elementary analysis of carbon, hydrogen, and nitrogen were carried out in a Perkin-Elmer device, model PE 2400. X-Ray Diffraction (XRD) was performed on a Shimadzu diffractometer, model XR-D600 A, in the 2θ range between 5 and 75 °. The scanning speed was 5 ° min^{-1}, using the CuKα radiation source, with a wavelength of 154.06 pm.

The hydrophilicity of the samples was determined by contact angle measurements with the water using the sessile drop method on the Theta instrument (Biolin Scientific) at 25.0 °C. In each membrane, a 4.0 ± 0.2 µL drop of water was deposited on the sample surface, and the video recorder was used to observe the interaction between the drop of water and the surfaces of the membranes for 1 minute. Analyzes were performed in quadruplicate.

2.4 Degree of porosity and thickness of the membranes

The degree of porosity of the membranes was measured by determining the amount of ethanol absorbed after 1 h of immersion in this solvent, using Equation (1) [32]:

$$P(\%) = \frac{W_2 - W_1}{d_{ethanol} \cdot V_{membrane}} \; x \; 100 \qquad \text{Eq. (1)}$$

where, W_1 represents the weight of the dry membrane and W_2 is the weight of the wet membrane, $d_{ethanol}$ the density of ethanol 100% (v/v) at room temperature, and $V_{membrane}$ is the volume of the membrane. To calculate the volume of the membrane, the radius was measured with a digital caliper (Mitutoyo, Japan) and the thickness was measured with a device for thickness measurement (Adamel Lhomargy, MI20, France).

2.5 Swelling Degree

The degree of swelling of the membranes was measured by the gravimetric method [33]. The membranes, approximately 0.87 cm in diameter, were dried at 45 °C for 1 h and weighed on an analytical balance. Then, they were immersed in PBS solution at room temperature for 1 h. After this period, the membranes were removed from the PBS solution and the excess was removed with filter paper before being weighed. The degree of swelling of each sample was performed in quadruplicate and calculated from the following Equation (2):

$$Swelling\ degree\ (\%) = \frac{W_f - W_0}{W_0} \; x \; 100 \qquad \text{Eq. (2)}$$

where, W_0 is the initial dry weight of the membrane and W_f is the swollen weight of the membrane after absorbing the PBS solution for 1 h.

2.6 Mechanical tests

Mechanical tests were performed on texturometer equipment (TA.XT plus Texture Analyzer, Stable Micro Systems, Cardiff, UK). Force calibration for a 5 Kg load cell was performed using a 2 Kg weight, and height calibration was performed using the film support rig and corresponding probe. The thickness of each sample was measured with a Micrometer MI 20 (Adamel Lhomargy, France). All analyzes were done at room temperature, ca. 25 ºC, and the maximum resistance to rupture of the membranes was calculated in quintuplicate.

2.7 Antileishmanial activity and Microscopy (AFM) analysis

The assay was performed with promastigote forms of *L. amazonensis* (IFLA/BR/67/PH 8) in logarithmic growth phase. The parasites were seeded in 96-well cell culture plates containing supplemented Schneider medium, in the amount of 1×10^6 leishmania/100.0 µL of medium. Then, the membranes were added to the wells in duplicate and serial dilutions were made, reaching six ranges of final concentrations (13 to 0.4 $\mu mol.L^{-1}$). The plate was incubated in a Biochemical Oxygen Demand (BOD) oven at a temperature of 26 °C for 48 h, with 6 h remaining for the end of this period, 20.0 µL of resazurin 1×10^{-3} $mol.L^{-1}$ were added. The absorbance reading was performed on a plate reader (Biotek, model ELx800), at a wavelength of 550 nm, and the results were expressed in terms of growth inhibition (%).

Microscopy (AFM) analysis of the treated and untreated *Leishmania amazonensis* used samples fixed with glutaraldehyde (2%), after the previously mentioned experiment.

Then, the samples were washed 3× with PBS (0.1 $mol.L^{-1}$) by centrifugation (1100 × g for 10 min at room temperature, ca.25 °C). The washed samples were placed (30.0 µL) on a clean glass slide. After the drying time, the slides were washed twice with distilled water and placed to dry again [34]. The study was carried out on TT-AFM equipment (AFM, Workshop, USA) in vibrating mode (tapping mode) with silicon cantilever (TAP300-G10, TED PELLA, INC) and resonance frequency of approximately 240 kHz. Images of 29 × 29 µm with resolution of 512 × 512 pixels were obtained and the images were processed using the Gwyddion 2.55 software.

2.8 Antioxidant activity

The ABTS [2,2-azino-bis(3-ethylbenzotiazoline-6-sulphonic acid)] assay was carried out according to Policarpi *et al.* [35] with modifications. Briefly, the ABTS radical (7.0 $mmol.L^{-1}$ – 0.0384 g ABTS, dissolved in 10.0 mL deionized water) was mixed with potassium persulfate (2.44 $mmol.L^{-1}$ – 10.0 mL and 10.0 mL ABTS persulfate), the solution was homogenized and stored in an amber flask in the dark for a minimum of 16 h. The ABTS solution was diluted with methanol to achieve an absorbance value of (0.700 ± 0.020) at 734 nm. Then 20.0 µL of extract stock solutions were added in 180.0 µL of adjusted ABTS solution and after 5 min the absorbance at 734 nm was determined with a microplate reader (Synergy H1, Vermont, USA). Trolox was used as the standard. The analysis was performed in triplicate, and the results were expressed as a percentage of reduction in absorbance compared to the control.

2.9 Biocompatibility in fibroblasts and keratinocytes

The cytotoxicity of MQC and MDHB was assessed through the cell viability of murine fibroblasts - L929 and human keratinocytes - HaCaT using the MTT assay following the standardized instructions according to ISO 10993-5.

HaCaT and L929 cell lines were seeded (1×10^4 cells/well) in 96-well microplates, maintained in DMEM supplemented with 20% and 10% (v/v) fetal bovine serum (FBS), respectively, and 1% (v/v) of antibiotics (penicillin/streptomycin/amphotericin B - Lonza, USA). Simultaneously, the extracts of the MQC and MDHB samples were prepared by adding 5.0 mg of each material to 1.0 mL of DMEM followed by incubation at 37 °C for 24 h.

After the cells reached subconfluence inside the wells, the culture media were carefully removed and replaced with MQC and MDHB extracts at concentrations of 39.06, 78.12, 156.25, 312.50, 625.00, 1250.00, 2500.00, and 5000.00 $\mu g.mL^{-1}$. After incubation for 24 h, the extracts were replaced with 50.0 µL of 1.0 $mg.mL^{-1}$ MTT solution, prepared in DMEM without supplements, and incubated again for another 2 h. Then, the MTT was replaced with 100.0 µL of DMSO and the microplate was stirred for about 10 min, until the formazan was completely solubilized. After that, the optical density at 570 nm was measured using a microplate reader (Multiskan Sky, Thermoscientific).

As a positive control of cytotoxicity, DMEM medium was added with 20% DMSO. As a negative control, of non-cytotoxic material, DMEM plus FBS and antibiotics were used. The values of optical density (OD) obtained were converted into percentages of relative cell viability of the sample and the negative control. All tests were performed in triplicate and in three independent experiments.

2.10 Morphological analysis of the fibroblasts

For each well of a 24-well plate, a disc of TCPS (Tissue Culture Polystyrene) was placed and, in sequence, L929 cells were sown in those wells (1×10^5 cells/well) in DMEM medium supplemented with 10% fetal bovine serum and 1% of antibiotics, and incubated at 37 °C and 5% of CO_2.

After this period, the culture medium was replaced by the extracts from the MQC and MDHB membranes at a concentration of 5000.0 $\mu g.mL^{-1}$ and the plate was incubated again, under the same conditions as the previous experiment, for 24 h. The extracts were removed, the TCPS membranes were washed twice with PSB, and then the cells on the TCPS membranes were fixed with at 2.5% (v/v) glutaraldehyde, by remaining in contact with the glutaraldehyde solution for at least 1 h. Then, samples were washed by removing the glutaraldehyde solution and substituting by deionized water, remaining in contact for 10 min. Afterwards samples were dehydrated by replacing deionized water with a sequence of ethanol solutions with increasing concentration (30, 50, 70, 80, 90, and 100% (v/v)). Each solution was left in contact with the samples for 10 min before being replaced by the following concentration. After the final 10 min contact with absolute ethanol (which was performed twice), the ethanol was removed and two drops (enough to cover the entire sample) of hexamethyldisilazane (HMDS; Sigma-Aldrich, USA) were placed over the samples and promptly evaporated to dryness with a nitrogen stream. Dried samples were then placed in observation stubs (covered with double sided adhesive carbon tape – NEM tape, from Nisshin, Japan) and coated with gold/palladium using a Sputter Coater (Polaron, from Bad Schwalbach, Germany). Samples were analyzed in a scanning electron microscope (SEM; JSM-5600LV, from JEOL, Japan) and observations were performed in high-vacuum with an acceleration voltage of 15 kV.

2.11 Wound Healing Assay

To determine whether MQC and MDHB could alter the rate of cell migration in HaCaT and, consequently, in wound healing, a scratch test was performed. This assay was carried out as described by Pinto *et al.* [36] with some modifications. Briefly, 24-well plates were seeded in DMEM medium supplemented with 10% Fetal Bovine Serum (SFB) and 1% antibiotics (penicillin/streptomycin/amphotericin B), 500.0 µL of a cell concentration of 2.0×10^5 cells.mL^{-1}, and the plates were incubated in BOD at 37 °C and 5% CO_2 until cell confluence was reached in all wells. When the confluence was reached, the culture medium was removed, then a vertical scratch was made in each well using a 200 µL tip, the cell monolayer was washed with 500.0 µL of PBS to remove cell fragments. The sample extracts were added at a concentration of 1.0 mg.mL^{-1}, and the cells were incubated again under the same conditions previously described. The extracts were obtained as described in the biocompatibility assay section, at the concentration of 1.0 mg.mL^{-1}. The cells treated with supplemented culture medium were used as controls. Wound closure was monitored through photographs taken at 0, 24, and 48 h using a Moticam 1 camera (1280 × 720 pix) attached to the lens of an inverted microscope (Axiovert 40 CFL Trinocular), observing the cells with the 10× objective. The percentage of wound closure, which reflects the rate of cell migration, was calculated based on the spider widths determined using the ImageJ 1.52a software, according to Equation 3:

$$Percent\ closure\ (\%) = \frac{(initial\ scratch\ width) - (final\ scratch\ width)}{initial\ scratch\ width}\ x\ 100 \qquad \text{Eq. (3)}$$

The width averages were obtained with 10 measurements along the entire scratch. The average of the initial width was that measured at t = 0 h, while the average of the final width was that measured at 24 or 48 h. Three independent experiments were carried out, each in quadruplicate.

2.12 Statistical analysis

For the biological tests, ANOVA analysis of variance was performed followed by the Bonferroni test in Graph Pad Prism 5.0, taking the value of $p < 0.05$ as the maximum level of statistical significance (95% confidence). For the other tests, the unpaired Student t test was employed.

3. RESULTS AND DISCUSSION

3.1 Physicochemical characterization

Elementary analysis was used to investigate the chemical composition of each sample. All the results of the elementary analysis of the membranes, expressed in percentages and amounts in mmol.g^{-1} of carbon, nitrogen, and hydrogen, as well as the carbon and nitrogen ratio, are listed in **Table 1.**

Table 1 - Percentages of carbon (C), hydrogen (H), and nitrogen (N) and the molar quantities of these elements for MQC and MDHB.

Sample	%			mmol.g^{-1}			C/N
	C	H	N	C	H	N	
MQC	38.55±0.14	8.56±0.29	6.34±0.07	32.13±0.12	85.60±2.90	4.53±0.05	7.09±0.10
MDHB	39.80±0.25	8.72±0.12	6.29±0.02	33.17±0.21	87.20±1.27	4.49±0.01	7.38±0.02

Initially, the MQC membrane presented 32.13 mmol.g^{-1} of carbon to 4.53 mmol.g^{-1} of nitrogen. With the insertion of the substance 2,3-DHB in the membrane to form the MDHB membrane, as expected, the amount of nitrogen did not vary, but the carbon changed to 33.17 mmol.g^{-1} causing the C/N ratio to increase from 7.09 to 7.38 mmol.g^{-1}. This increase occurred due to the presence of the new compound in the membrane indicating its successful incorporation in the polymeric matrix.

Infrared spectroscopy, as well as other spectroscopic techniques, were used to examine the formation of the membrane and the incorporation of 2,3-DHB. **Fig.1A** presents the MQC and MDHB spectra.

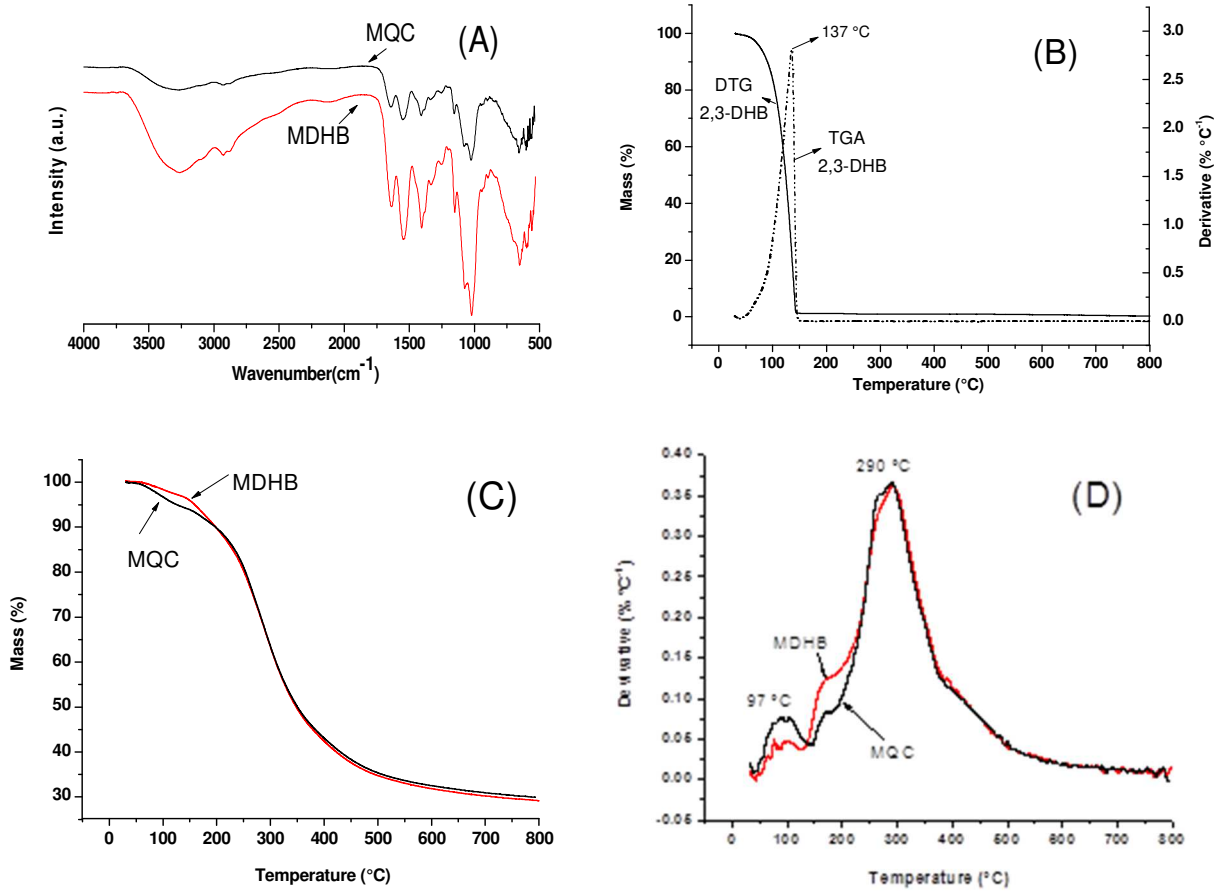

Figure 1 - Infrared spectra of MQC and MDHB (A); 2,3-DHB TG and DTG curves (B); TG (C), DTG (D) curves of MQC and MDHB. (Melhorar a figura 1.d)

The FTIR spectrum of the MQC membrane showed a characteristic profile of polysaccharide materials, consisting of chitosan and collagen, with bands around 3258 cm^{-1} (Amide A), 1635 cm^{-1} (Amide I), 1536 cm^{-1} (Amide II), and 1069 cm^{-1} (COC of the polysaccharide structure) [30,37,38]. This indicates that the presence of collagen in the chitosan membrane does not cause any significant change in chemical group oscillations [39,40]. In the process of synthesizing this membrane, the collagen and chitosan were

dissolved in an acid medium, with ionization of the carbonyl groups of the collagen and amine of the chitosan, producing an electrolytic reaction and interaction by electrostatic attraction between them [30]. The binding occurred in the amino groups of chitosan and collagen, belonging to amines I and II. Furthermore, carbonyl and collagen NH_2 groups can form these same bonds with OH and NH_2 groups of chitosan [37].

The FTIR spectrum of the MDHB membrane displayed an increase in band intensity around 3258 cm^{-1}, referring to the OH stretching of free water and the NH stretching of amide A [18,41]. The appearance of new bands in the region between 2857 and 2893 cm^{-1} and at 1397 cm^{-1} refer to the aromatic ring present in the structure of 2,3-DHB [42]. The bands related to the collagen triple helix are at 1635 cm^{-1} (Amide I), 1536 cm^{-1} (Amide II), and at 1250 cm^{-1} (Amide III) [43,44], which is very important because all the biological activity of collagen, including cell adhesion, depend on the structure of the triple helix [45].

The interaction between 2,3-DHB and the matrix can be observed in the figure below (Fig. 2). 2,3-DHB, which has an epoxide ring in its structure, is reactive due to ring tension. In an acidic environment, the oxygen in the epoxide is protonated and can then be attacked by the nucleophiles present in chitosan (-OH, -NH2). The more substituted carbon is more likely to be attacked, because a more substituted carbocation is more stable. The product showed an increase in the number of hydroxyls (-OH) and C-O bonds. Corroborating the increase in band intensities observed in the FTIR spectrum. The presence of more hydroxyls in the structure also implies an increase in the hydrophilicity of the material.

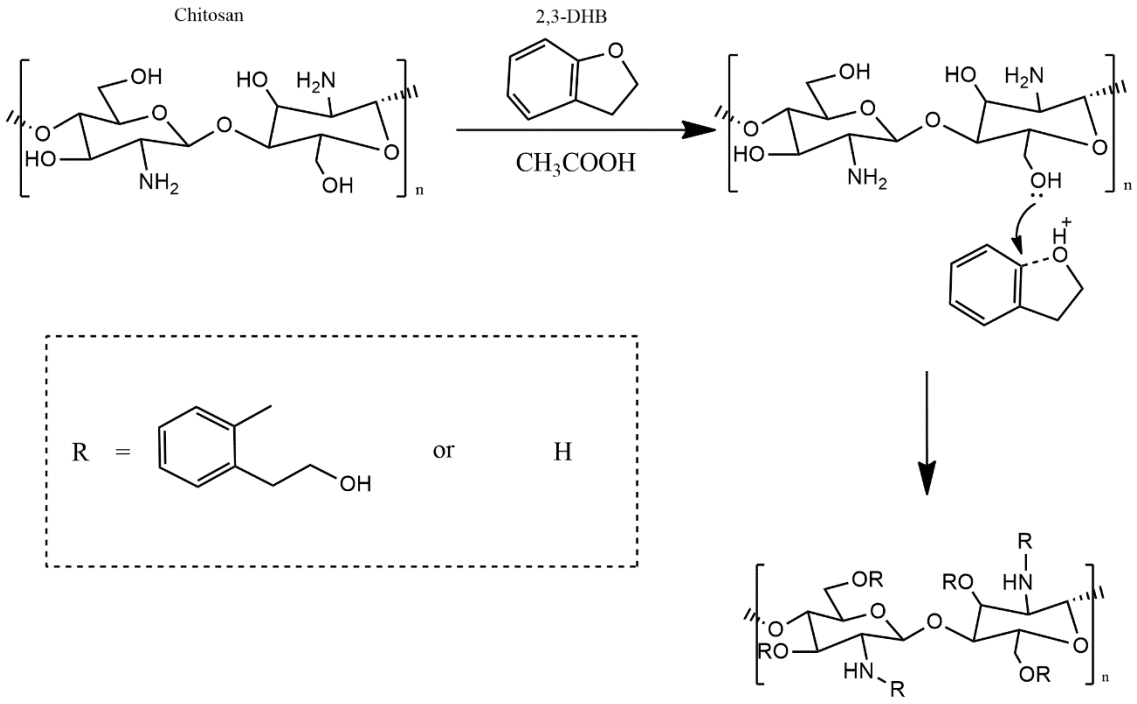

Figure 2 – Simplified scheme of the interaction of 2,3 DHB with chitosan.

Through thermogravimetric analysis (TG), an additional confirmation of the insertion of the 2,3-DHB molecular structure in the new membrane was sought, in addition to seeking to better understand their thermal stability. The TG and DTG curves of the pure 2,3-DHB (**Fig. 1B**) evidenced that it degraded in a single step. In this mass loss event, which occurred between 45 °C and 148 °C, with a maximum peak of DTG at 137 °C, all the material was degraded.

In thermogravimetric analyzes of the membranes (Fig. 1C and Fig. 1D) it was possible to notice that the first mass loss event, which is related to the loss of structurally bound water in the membranes, began at 50 °C for both MQC and MDHB. This event had a maximum dehydration peak at approximately 97 °C for both membranes. Likewise, it was possible to notice that the maximum decomposition peak of these membranes was also similar (approximately 290 °C). These high decomposition temperatures are important for future applications.

The thermogravimetric analysis of the membranes illustrated an additional increase of a small event in MDHB between 126 – 204 °C, evidenced by a small shoulder on the TG curve and a small peak in the DTG of this membrane for degradation of 2,3-DHB grafted to MDHB. The temperature increases related to the degradation of 2,3-DHB inserted in the membrane (170 °C), compared to pure 2,3-DHB (137 °C), suggests good interaction between this substance and the polymeric matrix.

The results of DSC analysis of pure 2,3-DHB, MQC, and MDHB are provided in **Fig. 3A.**

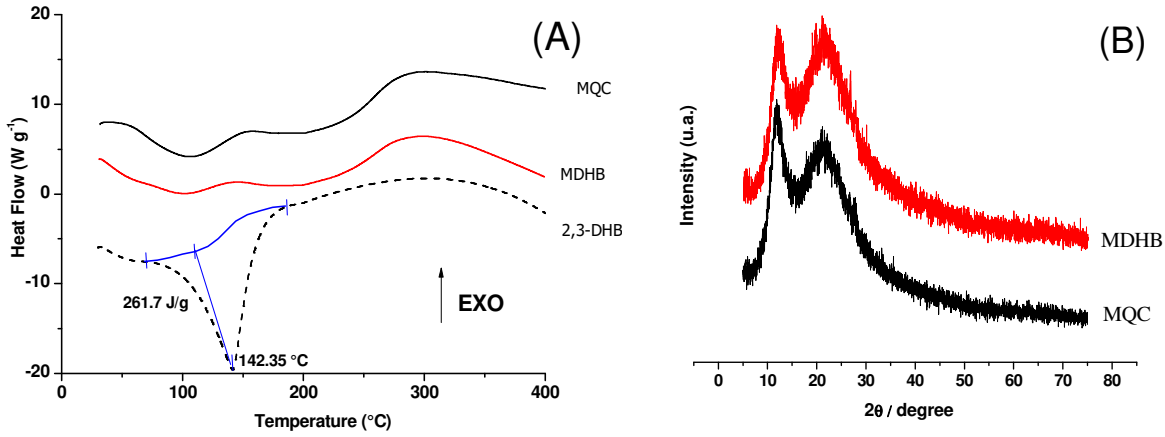

Figure 3 - DSC (A) and XRD (B) curves of MQC and MDHB.

The endothermic peak at around 100 °C for both MQC and MDHB was due to dehydration of these materials [46,47]. An accentuated endothermic peak is visible for 2,3-DHB at 142.35 °C, due to the degradation of the substance, but this peak is not observed in the MDHB membrane that carries the compound. This result suggests a uniform and amorphous dispersion at the molecular level of 2,3-DHB into the membrane matrix [48,49]. The MQC and MDHB membranes exhibited another endothermic peak above 150 °C. Comparing this event in the two membranes elucidates an increase in the

enthalpy variation in the MDHB membrane (MQC = 63.31 $J.g^{-1}$ and MDHB = 81.95 $J.g^{-1}$). The increase in energy involved in this endothermic event is related to the insertion of 2,3-DHB in the structure of the MQC membrane, indicating a structural difference between the membranes before and after the insertion of 2,3-DHB. DSC analysis verified that in the MQC and MDHB membranes the structure of the collagen triple helix was preserved without deformation, corroborating with the FTIR results. The endothermic peak of pure collagen, which occurs up to a temperature of 150 °C, was similar to that found in the manufactured membranes [30,50].

Fig. 3B illustrates the X-ray diffraction of the membranes. In MQC, the two largest peaks of chitosan diffraction in the microcrystalline state were found at 11.5° and 21.6° [22,51,52]. This last broad peak at 21.6° is also characteristic of collagen maintaining the integrity of its triple helix, corroborating with observation with FTIR and DSC [43,53,54]. In the MDHB membrane, the absence of a specific diffraction peak for 2,3-DHB confirms the uniform homogeneous dispersion of the substance in the polymeric matrix corroborating again with the DSC results [55].

The porosity, swelling capacity, maximum stress at break, and thickness of the MQC and MDHB membranes were also characterized (**Fig.4).**

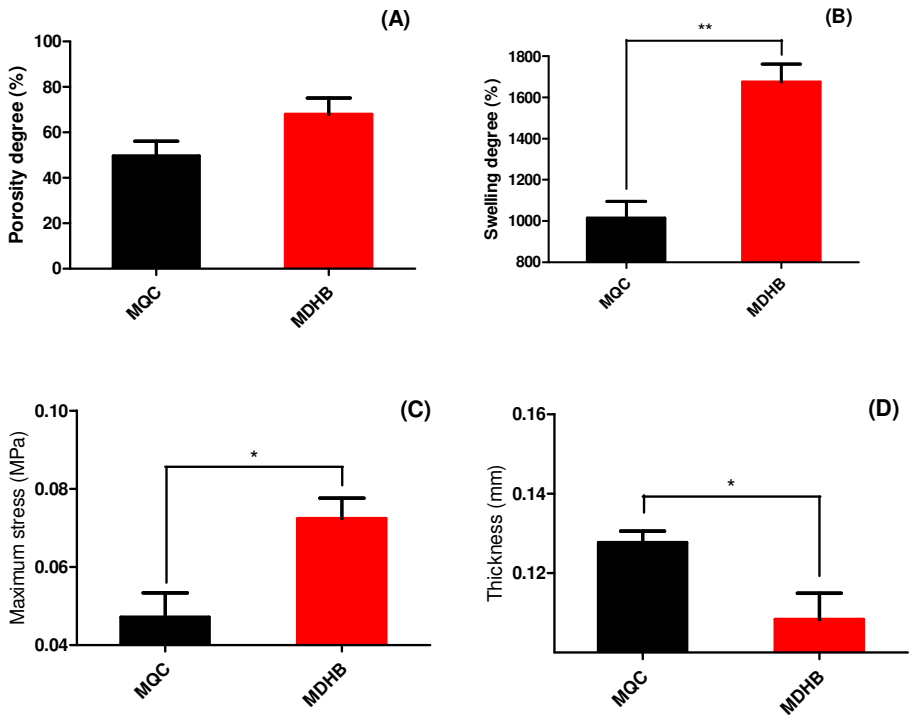

Figure 4 - Porosity (A), swelling (B), maximum tensile strength (C), and membrane thickness (D) MQC and MDHB (* $p < 0.05$ *and* ** $p < 0.01$ using unpaired Student's t-test, n = 5).

424

425 The porosity percentage of the MQC membrane was 49.51%, while that of the
426 MDHB membrane was 67.96%, as shown in **Fig.4A.** The addition of 2,3-DHB to the
427 structure of the chitosan and collagen membrane not only increased its porosity by
428 18.45%, but also fitted the MDHB membrane in the range of porosity considered ideal
429 for a wound dressing, which is from 60 to 90% [33]. Porosity is an important factor, as it
430 increases the surface area, promoting cell insertion and multiplication. In addition,
431 porosity determines mechanical properties and water retention, so that it can readily
432 absorb fluids present in a wound [37,40].

433 The increase in porosity of MDHB also increased the swelling capacity of this
434 membrane (**Fig.4B**). The swelling properties of biomaterials is strongly dependent on the
435 type and content of the polymers used. Biomaterials manufactured with collagen can have
436 characteristics such as high porosity associated with high water absorption capacity

[56,57], making it a suitable material for use in the medical device industry. Chitosan is also a biopolymer that has a high absorption capacity. Pallela, *et al.* [58] produced biomaterials based on chitosan and chitosan/collagen with absorption capacity of 2400% and 1000%, respectively. Xie *et al.* [59] produced wound dressing materials based on chitosan/collagen with swelling capacity greater than 1000% both in saline solution and in deionized water and PBS. The MDHB membrane showed a 661% increase in its swelling capacity in comparison to MQC, probably due to other water-binding groups after grafting the 2,3-DHB substance.

The maximum tensile strength measurements of the MQC and MDHB membranes are found in the **Fig. 4C**. The results showed that the properties varied with the use of the substance 2,3-DHB. The relatively high maximum burst stress exhibited by MDHB (0.07 Mpa) compared to MQC (0.05 Mpa) may be due to the increased number of ionic interactions with the insertion of the 2,3-DHB structure in the membrane.

As previously reported by Susanto *et al.* [60], the membrane tensile strength of less than 1.0 MPa is due to its constituent elements being purely natural materials, without the use of additional crosslinking agents that could improve their mechanical properties. The thickness of the membrane can also interfere with its mechanical property. Valenzuela-Rojo *et al.* [37] produced membranes of chitosan and collagen by lyophilization with a maximum stress of 0.21 MPa, which is greater than those found for the membranes developed in the present study. However, the thickness of the membrane tested by those researchers was 1.98 mm, while the thicknesses of the MQC and MDHB membranes were 0.13 and 0.11 mm, respectively (**Fig.4D**). The smaller thickness of the MDHB membrane in relation to the MQC, associated with the increase in the maximum stress for the rupture of MDHB, evidences the influence of 2,3-DHB in improving the mechanical property of the membrane.

The hydrophilicity of the MQC and MDHB membranes was determined by water contact angle measurements performed through the sessile drop method, during a time period between 0 to 60 seconds. **Fig. 5** demonstrates a marked decrease of the contact angle as a function of time.

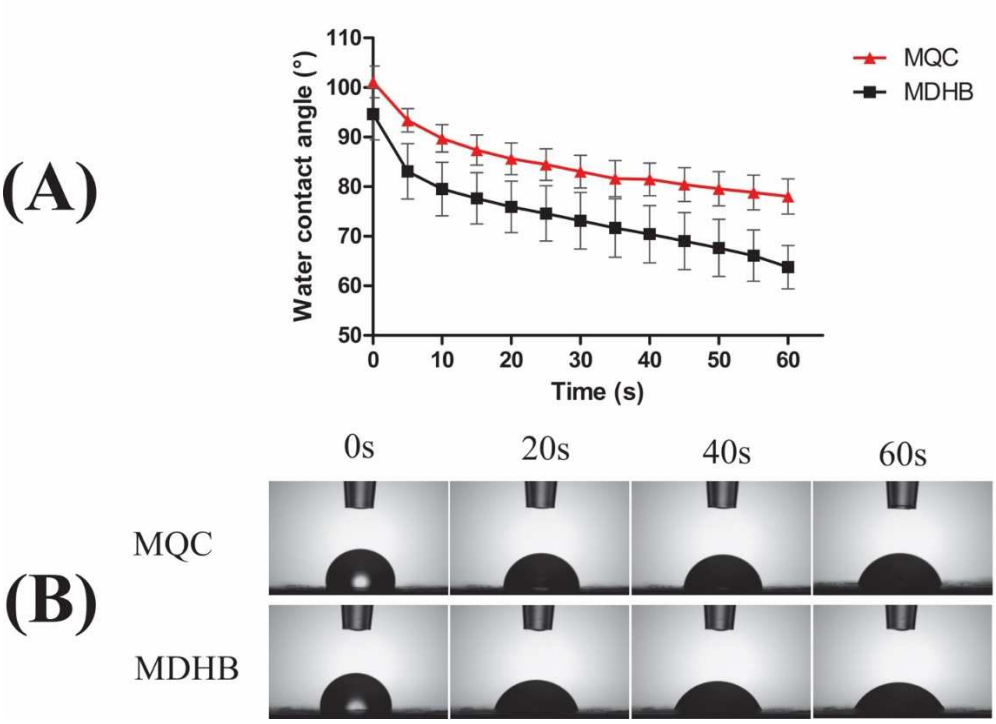

Figure 5 - (A) Curves of the averages of contact angles with water as a function of time and (B) images of water droplets as a function of time in the MQC and MDHB membranes.

This analysis evidences that the incorporation of 2,3-DHB caused an increase of the hydrophilicity in the membrane, which is an interesting factor for materials that are intended to be used in the treatment of wounds, greatly affecting the interaction between the biomaterial and the tissue, favoring the adhesion of fibroblasts and endothelial cells during healing [15,61].

3.2 Antioxidant activity

The antioxidant property of the membranes was determined by the ABTS radical scavenging method. This method is widely used to assess the antioxidant capacity of

476 different compounds [62]. The antioxidant capacity is reflected in the ability of the sample
477 to decrease the color, reacting directly with the radical ABTS. The MQC membrane
478 showed 25.77 ± 1.37%, while the MDHB membrane reduced 34.74 ± 1.30% in the ABTS
479 radicals. The presence of the 2,3-DHB substance provided an 8.97% increase in the
480 antioxidant capacity of the membrane.

481 The MQC membrane showed antioxidant activity due to chitosan. Pure chitosan
482 has previously reported antioxidant activity due to its amino and hydroxyl groups that
483 have the ability to reduce free radicals [63,64]. The MDHB membrane showed superior
484 antioxidant activity because 2,3-DHB is made up of a benzofuran ring structure. A series
485 of compounds based on benzofurans have antioxidant effects [65,66]. Furthermore, as
486 previously discussed, the inclusion of 2,3-DHB in the membrane promoted an increase in
487 available hydroxyl groups, which may also have contributed to the increase in antioxidant
488 activity. [67].

489

490 **3.3 Antileishmanial activity**

491 The inhibitory effect of MQC and MDHB membranes, the latter with
492 concentrations of 2,3-DHB ranging from 0.4 to 13 $\mu mol.L^{-1}$, on the promastigote form of
493 *L. amazonensis* can be observed in **Fig.6**.

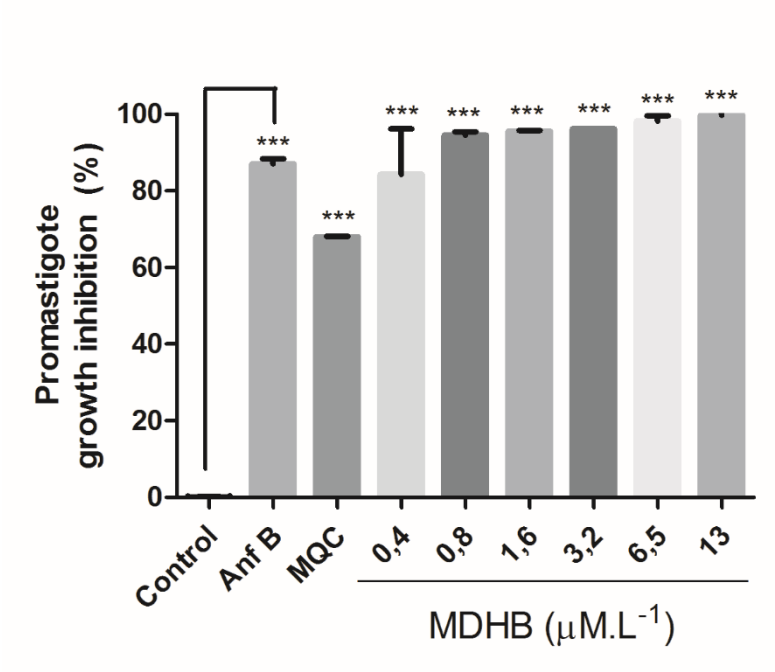

Figure 6 - Effect of MQC and MDHB against the promastigote form of *Leishmania amazonensis*. The figure represents the mean of the percentage ± standard error of the mean of the experiment carried out in duplicate. One-way ANOVA was performed to compare the groups with the control, with a significance level of *** p <0.001.

All membranes inhibited the growth of the parasite; however, the MDHB membranes were better than the MQC membrane, exhibiting greater antileishmanial effect. In addition, the MDHB membranes had inhibitory effects superior to the positive control (Amphotericin B). It was also observed that the inhibition of parasite growth was dependent on the concentration of 2,3-DHB in the membrane, exhibiting a dose-response effect in which the higher the concentration, the greater the inhibitory effect, reaching 100% growth inhibition at the concentration of 13 µmol.L^{-1}.

In the studies by Oliveira et al [9], 2,3-DHB alone at a concentration of 13 µmol.L^{-1} had an inhibited the growth of *L. amazonensis* by 86.76%, slightly lower than that of Amphotericin B (87.0%), but with the advantage of being more selective to the parasite. In the present study, the MDHB membrane presented an IC_{50} (0.081 µmol.L^{-1}) lower than

512 the IC_{50} of 2,3-DHB (1.042 µmol.L^{-1}), being effective as a leishmanicide in all
513 concentrations studied.

514 The 2,3-DHB was effective in decreasing the number of amastigote forms of *L.*
515 *amazonensis* internalized by macrophages, in addition to decreasing the number of
516 amastigotes per infected macrophage [9]. The developed membranes may have these
517 characteristics also improved, which make them excellent candidates for advanced *in vivo*
518 studies.

519 The atomic force microscopy images prove the efficiency of the new membrane
520 manufactured on the parasite of *Leishmania amazonensis.* **Fig.7A** shows the typical
521 morphology of the *Leishmania* promastigote form, in the form of a spindle with an
522 anterior flagellum, similar to that already described by AFM and SEM [34].

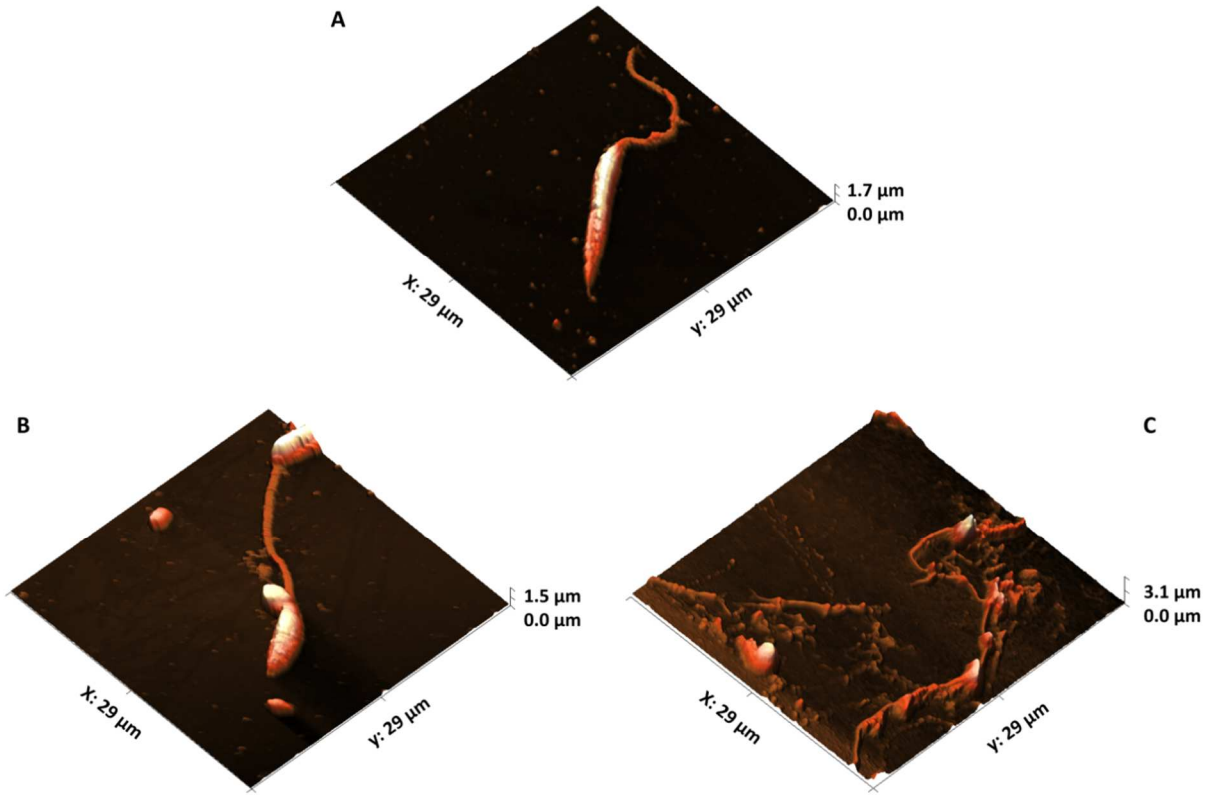

Figure 7 - Atomic Force Microscopy (AFM) of *Leishmania amazonensis* promastigote cells. AFM amplitude images of untreated (control) cell (A), cells treated with 2,3-DHB at a concentration of 13 µmol.L^{-1} (B), and with MDHB at a concentration of 13 µmol.L^{-1} (C).
523

In the AFM images of the cells treated with 2,3-DHB and with MDHB, considerable differences were found from the control. Disturbances occurred in cell body membranes, with less elongated cells after treatment with 2,3-DHB **(Fig.7B)**, proving that the substance has an action on the microorganism. In the treatment with the MDHB membrane, the cell body was not found, leaving only traces of the flagella **(Fig.7C)**. This result proves again the effectiveness of the new membrane developed here as a leishmanicidal agent.

The decrease in cell length, leading to an ovoid and round shape has already been described by Eaton *et al.* [34], when studying *Leishmania infantum* by AFM and SEM, as being associated with the rupture of the membrane, indicating that 2,3-DHB acts directly on the parasite's membrane, causing its death.

3.4 Biocompatibility

The cytotoxic effects of the MQC and MDHB membranes were investigated by the MTT assay in fibroblasts - L929 and in keratinocytes - HaCaT (**Fig.8A-B**). These cell lines were chosen because they represent cells present in the skin and participate in the wound healing process [68,69]. In addition, SEM micrographs of fibroblasts treated with the MDHB membrane (**Fig.8C**) were compared with the control (**Fig.8D**).

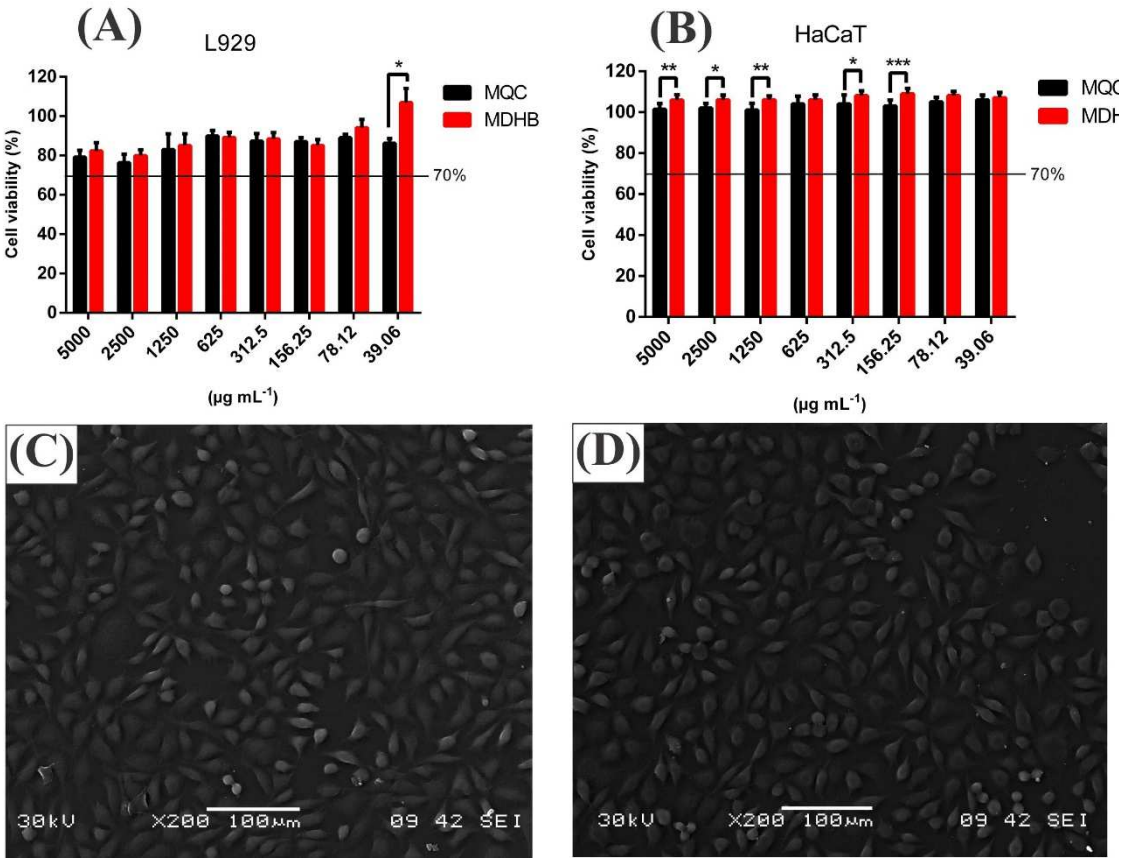

Figure 8 – Cell viability of fibroblasts - L929 (A) and keratinocytes – HaCaT (B) treated with MQC and MDHB by the MTT assay. Scanning electron microscopy (SEM) of fibroblasts - L929 not treated (C) and treated (D) with MDHB. In A and B, cell viability is represented by the mean ± standard error of the experiment average performed in triplicate. One-way ANOVA was performed to compare groups with the control, with * p <0.05, ** p <0.01 and *** p <0.001.

In L929 (**Fig.8A**), cell viability was greater than 70%, for both MQC and MDHB, for all concentrations tested, being higher than 80% for almost all concentrations, thus in compliance with ISO 10993-5 [70]. These results are in agreement with other studies carried out both *in vitro* and *in vivo*, which in addition to confirm the non-cytotoxicity of chitosan/collagen membranes with fibroblasts, also evidence that biomaterials constituted of these biopolymers stimulate its proliferation in wounds [15,60]. In addition, SEM micrographs of fibroblasts treated with the MDHB membrane (**Fig.8D**) found no morphological change in the cells when compared with the control (**Fig.8C**), as they

maintained their characteristic triangular shape, which reinforces the concept that membranes are not cytotoxic.

The MQC and MDHB membranes also did not show cytotoxicity in human keratinocytes (HaCaT). As it can be seen in **Fig.8B**, the membranes stimulated cell proliferation in this lineage, obtaining a percentage of cell viability greater than 100% for all concentrations tested. When comparing the cell viability of the keratinocytes treated with the membranes, in all concentrations, the cell viability values of MDHB were higher than those of MQC, indicating that the addition of 2,3-DHB to the membrane stimulated cell proliferation in that lineage. As seen previously, the MDHB membranes maintained the triple collagen helix and exhibited greater antioxidant activity than the MQC membranes. This increase in antioxidant activity may have been responsible for the increase in cell proliferation observed, since antioxidant substances may increase cell proliferation in keratinocytes by providing a decrease in oxidative stress and or by stimulating the intracellular activity of superoxide dismutase, a primary antioxidant enzyme that catalyzes the dismutation reaction of the superoxide radical [71]. The maintenance of the triple helix could be another factor responsible for the increase in cell proliferation since all biological properties are dependent on its structure. The proliferation of skin cells is important for the proper healing of wounds after injuries. These results suggest, therefore, that the MDHB membrane, in addition to improving the antileishmanial effect, can also increase the potential for skin tissue healing and regeneration.

3.4 Wound healing assay

Wound healing is a complex process that involves the integrated response of different cells and growth factors and results in the renewal of the structure and function

of the skin [72]. Chitosan and collagen are active materials for wound healing. Some studies show that these materials accelerate healing, by stimulating cell proliferation, in addition to preventing the development of infections [20,73,74]. In this work, after the biocompatibility tests indicated their potential for wound healing and regeneration, the cell migration capacity was tested in keratinocytes (HaCaT) treated with the formulated membranes by performing an *in vitro* wound healing test (**Fig 9B**). The evolution of the recovered wound area is illustrated in **Fig. 9A**.

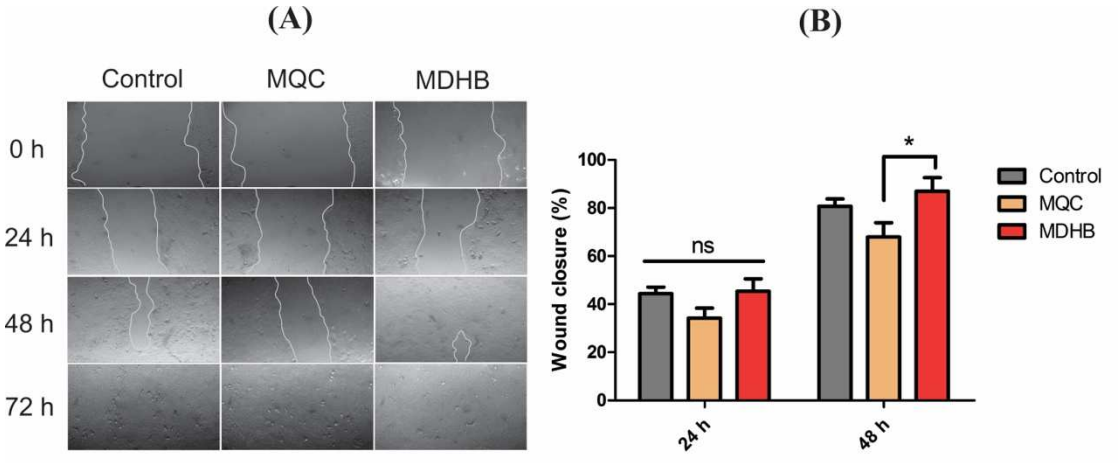

Figure 9 - Representative micrographs of wounds on human keratinocytes (HaCaT) treated with MQC, MDHB, and control at different time intervals (A). Percentage of wound closure in the control cells, MQC and MDHB at different time intervals (B). The results are expressed as mean ± standard error of three independent experiments performed in quadruplicate; * p <0.05; ns indicates that there was no significant difference between treatments. The percentage of wound closure was calculated using the Image J software.

As shown in **Fig. 9A**, the tendency of the treated groups to close the wound was assessed by the movement of the cells to fill the scratched area. In 24 h, the scratch of the wounds treated with MQC, MDHB, and control exhibited a moderate degree of cell migration resulting in partial wound closure, with no difference between materials. As early as 48 h after the wound was made, HaCaT cells treated with the MDHB membrane did not show significant differences in relation to the control, but exhibited a distinct

wound healing effect compared to cells treated with the MQC membrane, as they migrated more quickly, with a migration rate about 19% higher, followed by complete closure of the wound after evaluation in 72 h. Wound closure was complete for both materials in 72 h along with the control. These results demonstrate that the MDHB membrane creates an adequate environment for cell proliferation and growth.

Considering the healing capacity of human keratinocytes (HaCaT), as well as the absence of cytotoxicity of the formulated membrane, the present work constitutes a promising approach for the *in situ* treatment of cutaneous Leishmaniasis, which will be validated with further investigation *in vivo.*

4. CONCLUSION

In the present work a new chitosan/collagen-based membrane incorporating 2,3-DHB was successfully developed, maintaining the collagen integrity preserved without deformation. The presence of the antileishmanial agent in the new membrane have resulted in better mechanical properties and induced higher porosity, swelling capacity, hydrophilicity and antioxidant activity. The antileishmanial activity tests against the promastigote form of *Leishmania amazonensis* exhibited inhibitory effects superior to those of Amphotericin B, which is used in the treatment of Leishmaniasis. It also presented biocompatibility with L929 cells and stimulated the proliferation of HaCaT cells. The healing tests demonstrated that the MDHB membrane has a suitable environment for cell migration and growth. These results evidence that the formulated membrane is a great candidate to be used in the treatment of cutaneous Leishmaniasis, being indicated for advanced studies *in vivo*.

ACKNOWLEDGMENTS

The authors thank the Federal University of Piauí (UFPI) and the School of Biotechnology of the Center for Biotechnology and Fine Chemistry (CBQF) of the Catholic University of Porto for providing work research conditions (National Funds from FCT - Fundação para a Ciência e a Tecnologia through project UID/Multi/50016/2019). This study was financed in part by the Higher Education Improvement Coordination - Brasil (Capes) - Finance Code 001, and the Brazilian National Council for Scientific and Technological Development (306176/2019-0; 408635/2016-9 and 307460/2016-9).

REFERENCES

[1] Organização Pan-Americana da Saúde, Leishmanioses: Informe Epidemiológico das Américas, Informe de Leishmanioses Nº 7 1 (2019) 1–27.

[2] C.N. Dias, T.A.L. Nunes, J.M.S. Sousa, L.H. Costa, R.R.L. Rodrigues, A.J. Araújo, J.D.B. Marinho Filho, M.V. Silva, M.R. Oliveira, F.A.A. Carvalho, K.A.F. Rodrigues, 2020. Methyl gallate: Selective antileishmanial activity correlates with host-cell directed effects. Chem. Biol. Interact. 320, 109026. https://doi.org/10.1016/j.cbi.2020.109026.

[3] A.L.S. Santos, F.P. Matteoli, D.S. Gonçalves, S.H. Seabra, M.T. V. Romanos, M.H. Branquinha, G.O. Resende, B.A. Cotrim, L.C.S. Aguiar, L.S. Sangenito, 2019. In vitro effects of the asymmetric peptidomimetic 157, containing L-tartaric acid core and valine/leucine substituents, on Leishmania amazonensis promastigotes and amastigotes. Parasitol. Int. 73, 101968. https://doi.org/10.1016/j.parint.2019.101968.

[4] J.P.B. Menezes, C.E.S. Guedes, A.L.O.A. Petersen, D.B.M. Fraga, P.S.T. Veras, 2015. Advances in development of new treatment for leishmaniasis, Biomed. Res. Int. 2015, 815023. https://doi.org/10.1155/2015/815023.

[5] A.A.L. Sepúlveda, A.M.A. Velásquez, I.A.P. Linares, L. Almeida, C.R. Fontana, C. Garcia, M.A.S. Graminha, 2020. Efficacy of photodynamic therapy using TiO2 nanoparticles doped with Zn and hypericin in the treatment of cutaneous Leishmaniasis caused by Leishmania amazonensis. Photodiagnosis Photodyn. Ther. 30, 101676. https://doi.org/10.1016/j.pdpdt.2020.101676.

[6] L.A. Carneiro, T.V. Santos, L.V. do R. Lima, P.K.S. Ramos, M.B. Campos, F.T. Silveira, 2020. First report on feline leishmaniasis caused by Leishmania (Leishmania) amazonensis in Amazonian Brazil. Vet. Parasitol. Reg. Stud. Reports. 19, 100360. https://doi.org/10.1016/j.vprsr.2019.100360.

[7] L. Firmino-Cruz, T.D. Ramos, A.M. Fonseca-Martins, D. Oliveira-Maciel, G. Oliveira-Silva, J.S. Santos, C. Cavazzoni, A. Morrot, D.C.O. Gomes, A.M. Vale, D. Decoté-Ricardo, C.G. Freire-de-Lima, H.L. de M. Guedes, 2020. B-1 lymphocytes are able to produce IL-10, but is not pathogenic during Leishmania (Leishmania) amazonensis infection. Immunobiology. 225, 151857. https://doi.org/10.1016/j.imbio.2019.10.006.

[8] P. Scott, F.O. Novais, Cutaneous leishmaniasis: Immune responses in protection and pathogenesis, Nat. Rev. Immunol. 16 (2016) 581–592. https://doi.org/10.1038/nri.2016.72.

[9] L.G. de C. Oliveira, L.M. Brito, M.M. de M. Alves, L.V. Amorim, E.P.C. Sobrinho-Júnior, C.E.S. Carvalho, K.A. da F. Rodrigues, D.D.R. Arcanjo, A.M. das G.L. Citó, F.A. de A. Carvalho, In Vitro Effects of the Neolignan 2,3-Dihydrobenzofuran Against Leishmania Amazonensis, Basic. Clin. Pharmacol. Toxicol. 120 (2017) 52–58. https://doi.org/10.1111/bcpt.12639.

[10] A. Veeruraj, M. Arumugam, T. Ajithkumar, T. Balasubramanian, Isolation and characterization of collagen from the outer skin of squid (Doryteuthis singhalensis), Food Hydrocoll. 43 (2015) 708–716. https://doi.org/10.1016/j.foodhyd.2014.07.025.

[11] L. Fan, J. Yi, J. Tong, X. Zhou, H. Ge, S. Zou, H. Wen, M. Nie, Preparation and characterization of oxidized konjac glucomannan/carboxymethyl chitosan/graphene oxide hydrogel, Int. J. Biol. Macromol. 91 (2016) 358–367. https://doi.org/10.1016/j.ijbiomac.2016.05.042.

[12] O. Akturk, A. Tezcaner, H. Bilgili, M.S. Deveci, M.R. Gecit, D. Keskin, Evaluation of sericin/collagen membranes as prospective wound dressing biomaterial, J. Biosci. Bioeng. 112 (2011) 279–288. https://doi.org/10.1016/j.jbiosc.2011.05.014.

[13] M. Li, M. Han, Y. Sun, Y. Hua, G. Chen, L. Zhang, Oligoarginine mediated collagen/chitosan gel composite for cutaneous wound healing, Int. J. Biol. Macromol. 122 (2019) 1120–1127. https://doi.org/10.1016/j.ijbiomac.2018.09.061.

[14] A.E. Sorkio, E.P. Vuorimaa-Laukkanen, H.M. Hakola, H. Liang, T.A. Ujula, J.J. Valle-Delgado, M. Österberg, M.L. Yliperttula, H. Skottman, Biomimetic collagen I and IV double layer Langmuir-Schaefer films asmicroenvironment for human pluripotent stem cell derived retinal pigment epithelial cells, Biomaterials. 51 (2015) 257–269. https://doi.org/10.1016/j.biomaterials.2015.02.005.

[15] M. Andonegi, K. Las Heras, E. Santos-Vizcaíno, M. Igartua, R.M. Hernandez, K. de la Caba, P. Guerrero, 2020. Structure-properties relationship of chitosan/collagen films with potential for biomedical applications. Carbohydr. Polym. 237, 116159. https://doi.org/10.1016/j.carbpol.2020.116159.

[16] Z. Ruszczak, Effect of collagen matrices on dermal wound healing, Adv. Drug Deliv. Rev. 55 (2003) 1595–1611. https://doi.org/10.1016/j.addr.2003.08.003.

[17] K.M. Pawelec, S.M. Best, R.E. Cameron, Collagen: A network for regenerative medicine, J. Mater. Chem. B. 4 (2016) 6484–6496. https://doi.org/10.1039/c6tb00807k.

[18] E.M.A. Braz, S.C.C.C. Silva, D.A. Silva, F.A.A. Carvalho, H.M. Barreto, L.S. Santos Júnior, E.C. Silva-Filho, Modified chitosan-based bioactive material for antimicrobial application: Synthesis and characterization, Int. J. Biol. Macromol. 117 (2018) 640–647. https://doi.org/10.1016/j.ijbiomac.2018.05.205.

[19] E.M.A. Braz, S.C.C.C. Silva, C.A.R.S. Brito, L.M. Brito, H.M. Barreto, F.A.A. Carvalho, L.S. Santos Jr, A.O. Lobo, J.A. Osajima, K.S. Sousa, E.C. Silva-Filho, 2020. Spectroscopic, thermal characterizations and bacteria inhibition of chemically modified chitosan with phthalic anhydride. Mater. Chem. Phys. 240, 122053. https://doi.org/10.1016/j.matchemphys.2019.122053.

[20] M.O.G. Ferreira, L.L.R. Leite, I.S. Lima, H.M. Barreto, L.C.C. Nunes, A.B. Ribeiro, J.A. Osajima, E.C. Silva Filho, Chitosan Hydrogel in combination with Nerolidol for healing wounds, Carbohydr. Polym. 152 (2016) 409–418. https://doi.org/10.1016/j.carbpol.2016.07.037.

[21] M.O.G. Ferreira, I.S. de Lima, A.Í.S. Morais, S.O. Silva, R.B.F. de Carvalho, A.B. Ribeiro, J.A. Osajima, E.C. Silva Filho, Chitosan associated with chlorhexidine in gel form: Synthesis, characterization and healing wounds applications, J. Drug Deliv. Sci. Technol. 49 (2019) 375–382. https://doi.org/10.1016/j.jddst.2018.12.003.

[22] L.A. Pereira, L. da Silva Reis, F.A. Batista, A.N. Mendes, J.A. Osajima, E.C. Silva-Filho, 2019. Biological properties of chitosan derivatives associated with the ceftazidime drug. Carbohydr. Polym. 222, 115002. https://doi.org/10.1016/j.carbpol.2019.115002.

[23] L.C.B. Lima, C.C. Coelho, F.C. Silva, A.B. Meneguin, H.S. Barud, R.D.S. Bezerra, C. Viseras, J.A. Osajima, E.C. Silva Filho, 2019. Hybrid Systems Based on Talc and Chitosan for Controlled Drug Release. Materials. 12, 3634. https://doi.org/10.1137/S0036139995293269.

[24] M. Rezaii, S. Oryan, A. Javeri, Curcumin nanoparticles incorporated collagen-chitosan scaffold promotes cutaneous wound healing through regulation of TGF-β1/Smad7 gene expression, Materials Science and Engineering C. 98 (2019) 347–357. https://doi.org/10.1016/j.msec.2018.12.143.

[25] D. Archana, B.K. Singh, J. Dutta, P.K. Dutta, Chitosan-PVP-nano silver oxide wound dressing: In vitro and in vivo evaluation, Int. J. Biol. Macromol. 73 (2015) 49–57. https://doi.org/10.1016/j.ijbiomac.2014.10.055.

[26] S.S. Behera, U. Das, A. Kumar, A. Bissoyi, A.K. Singh, Chitosan/TiO2 composite membrane improves proliferation and survival of L929 fibroblast cells: Application in wound dressing and skin regeneration, Int. J. Biol. Macromol. 98 (2017) 329–340. https://doi.org/10.1016/j.ijbiomac.2017.02.017.

[27] S. Kumar, J. Dutta, P.K. Dutta, Preparation and characterization of N-heterocyclic chitosan derivative based gels for biomedical applications, Int. J. Biol. Macromol. 45 (2009) 330–337. https://doi.org/10.1016/j.ijbiomac.2009.08.002.

[28] M. Li, M. Han, Y. Sun, Y. Hua, G. Chen, L. Zhang, Oligoarginine mediated collagen/chitosan gel composite for cutaneous wound healing, Int. J. Biol. Macromol. 122 (2019) 1120–1127. https://doi.org/10.1016/j.ijbiomac.2018.09.061.

[29] J. Si, Y. Yang, X. Xing, F. Yang, P. Shan, Controlled degradable chitosan / collagen composite scaffolds for application in nerve tissue regeneration, Polym. Degrad. Stab. 166 (2019) 73–85. https://doi.org/10.1016/j.polymdegradstab.2019.05.023.

[30] A. Alagha, A. Nourallah, S. Hariri, 2020. Characterization of dexamethasone loaded collagen-chitosan sponge and in vitro release study. J. Drug. Deliv. Sci. Technol. 55, 101449. https://doi.org/10.1016/j.jddst.2019.101449.

[31] A. Sionkowska, B. Kaczmarek, R. Gadzala-Kopciuch, Gentamicin release from chitosan and collagen composites, J. Drug Deliv. Sci. Technol. 35 (2016) 353–359. https://doi.org/10.1016/j.jddst.2016.09.001.

[32] B.P. Antunes, A.F. Moreira, V.M. Gaspar, I.J. Correia, Chitosan/arginine-chitosan polymer blends for assembly of nanofibrous membranes for wound regeneration, Carbohydr. Polym. 130 (2015) 104–112. https://doi.org/10.1016/j.carbpol.2015.04.072.

[33] M. Yin, Y. Wang, Y. Zhang, X. Ren, Y. Qiu, T.-S. Huang, 2020. Novel quaternarized N-halamine chitosan and polyvinyl alcohol nanofibrous membranes as hemostatic materials with excellent antibacterial properties. Carbohydr. Polym. 232, 115823. https://doi.org/10.1016/j.carbpol.2019.115823.

[34] P. Eaton, C.R. Bittencourt, V.C. Silva, L.M.C. Véras, C.H.N. Costa, M.J. Feio, J.R.S.A. Leite, Anti-leishmanial activity of the antimicrobial peptide DRS 01 observed in Leishmania infantum (syn. Leishmania chagasi) cells, Nanomedicine. 10 (2014) 483–490. https://doi.org/10.1016/j.nano.2013.09.003.

[35] P. de B. Policarpi, L. Turcatto, F. Demoliner, R.A. Ferrari, V.L.A.F. Bascuñan, J.C. Ramos, I. Jachmanián, L. Vitali, G.A. Micke, J.M. Block, Nutritional potential, chemical profile and antioxidant activity of Chichá (Sterculia striata) nuts and its by-products, Food Research International. 106 (2018) 736–744. https://doi.org/10.1016/j.foodres.2017.12.069.

[36] B.I. Pinto, N.D. Cruz, O.R. Lujan, C.R. Propper, R.S. Kellar, 2019. In Vitro Scratch Assay to Demonstrate Effects of Arsenic on Skin Cell Migration. J. Vis. Exp. 144, e58838. https://doi.org/10.3791/58838.

[37] R.D. Valenzuela-Rojo, J. López-Cervantes, D.I. Sánchez-Machado, A.A. Escárcega-Galaz, M. del R. Martínez-Macias, 2020. Antibacterial, mechanical and physical properties of collagen - chitosan sponges from aquatic source. Sustain. Chem. Pharm. 15, 100218. https://doi.org/10.1016/j.scp.2020.100218.

[38] X. Yu, L. Guo, M. Liu, X. Cao, S. Shang, Z. Liu, D. Huang, Y. Cao, F. Cui, L. Tian, Callicarpa nudiflora loaded on chitosan-collagen/organomontmorillonite composite membrane for antibacterial activity of wound dressing, Int. J. Biol. Macromol. 120 (2018) 2279–2284. https://doi.org/10.1016/j.ijbiomac.2018.08.113.

[39] A.L. Skwarczynska, D. Binias, W. Maniukiewicz, Z. Modrzejewska, T.E.L. Douglas, The mineralization effect on chitosan hydrogel structure containing collagen and alkaline phosphatase, J. Mol. Struct. 1187 (2019) 86–97. https://doi.org/10.1016/j.molstruc.2019.03.034.

[40] P. Jithendra, A.M. Rajam, T. Kalaivani, A.B. Mandal, C. Rose, Preparation and characterization of aloe vera blended Collagen-Chitosan composite scaffold for tissue engineering applications, ACS Appl. Mater. Interfaces. 5 (2013) 7291–7298. https://doi.org/10.1021/am401637c.

[41] N. Benbettaïeb, O. Chambin, A. Assifaoui, S. Al-Assaf, T. Karbowiak, F. Debeaufort, Release of coumarin incorporated into chitosan-gelatin irradiated films, Food Hydrocoll. 56 (2016) 266–276. https://doi.org/10.1016/j.foodhyd.2015.12.026.

[42] Y. Rajashekar, H.V. Kumar, K. V. Ravindra, N. Bakthavatsalam, Isolation and characterization of biofumigant from leaves of Lantana camara for control of stored grain insect pests, Ind. Crops Prod. 51 (2013) 224–228. https://doi.org/10.1016/j.indcrop.2013.09.006.

[43] H. Goodarzi, K. Jadidi, S. Pourmotabed, E. Sharifi, H. Aghamollaei, Preparation and in vitro characterization of cross-linked collagen – gelatin hydrogel using EDC/NHS for corneal tissue engineering applications, Int. J. Biol. Macromol. 126 (2019) 620–632. https://doi.org/10.1016/j.ijbiomac.2018.12.125.

[44] A.M. Abdel-Mohsen, R.M. Abdel-Rahman, I. Kubena, L. Kobera, Z. Spotz, M. Zboncak, R. Prikryl, J. Brus, J. Jancar, 2020. Chitosan-glucan complex hollow fibers reinforced collagen wound dressing embedded with aloe vera. Part I: Preparation and characterization. Carbohydr. Polym. 230, 115708. https://doi.org/10.1016/j.carbpol.2019.115708.

[45] J.M. Pachence, Collagen-based devices for soft tissue repair, J. Biomed. Mater. Res. 33 (1996) 35–40. https://doi.org/10.1002/(SICI)1097-4636(199621)33:1<35::AID-JBM6>3.0.CO;2-N.

[46] M. Gierszewska, J. Ostrowska-Czubenko, Chitosan-based membranes with different ionic crosslinking density for pharmaceutical and industrial applications, Carbohydr. Polym. 153 (2016) 501–511. https://doi.org/10.1016/j.carbpol.2016.07.126.

[47] M.J. Boggione, C.R.A. Mahl, M.M. Beppu, B. Farruggia, Synthesis and characterization of chitosan membranes functionalized with amino acids and copper for adsorption of endoglucanase, Powder Technol. 315 (2017) 250–257. https://doi.org/10.1016/j.powtec.2017.04.014.

[48] N. Nematidil, M. Sadeghi, S. Nezami, H. Sadeghi, 2019. Synthesis and characterization of Schiff-base based chitosan-g-glutaraldehyde/NaMMTNPs-APTES for removal Pb2+ and Hg2+ ions. Carbohydr. Polym. 222, 114971. https://doi.org/10.1016/j.carbpol.2019.114971.

[49] X. Huo, W. Li, Y. Wang, N. Han, J. Wang, N. Wang, X. Zhang, Chitosan composite microencapsulated comb-like polymeric phase change material via coacervation microencapsulation, Carbohydr. Polym. 200 (2018) 602–610. https://doi.org/10.1016/j.carbpol.2018.08.003.

[50] A. George, A. Veis, FTIRS in H2O Demonstrates That Collagen Monomers Undergo a Conformational Transition Prior to Thermal Self-Assembly in Vitro, Biochemistry. 30 (1991) 2372–2377. https://doi.org/10.1021/bi00223a011.

[51] R. Huang, W. Li, X. Lv, Z. Lei, Y. Bian, H. Deng, H. Wang, J. Li, X. Li, Biomimetic LBL structured nano fi brous matrices assembled by chitosan/collagen for promoting wound healing, Biomaterials. 53 (2015) 58–75. https://doi.org/10.1016/j.biomaterials.2015.02.076.

[52] L. Sun, J. Han, Z. Liu, S. Wei, X. Su, G. Zhang, The facile fabrication of wound compatible anti-microbial nanoparticles encapsulated Collagenous Chitosan matrices for effective inhibition of poly- microbial infections and wound repairing in burn injury care : Exhaustive in vivo evaluations, J. Photochem. Photobiol. B. 197 (2019) 111539. https://doi.org/10.1016/j.jphotobiol.2019.111539.

[53] G.C. Jayakumar, N. Usharani, K. Kawakami, J.R. Rao, B.U. Nair, Preparation of antibacterial collagen – pectin particles for biotherapeutics, RSC Adv. 4 (2014) 42846–42854. https://doi.org/10.1039/C4RA07683D.

[54] A. Maged, A.A. Abdelkhalek, A.A. Mahmoud, S. Salah, M.M. Ammar, M.M. Ghorab, Mesenchymal stem cells associated with chitosan scaffolds loaded with rosuvastatin to improve wound healing, European Journal of Pharmaceutical Sciences. 127 (2019) 185–198. https://doi.org/10.1016/j.ejps.2018.11.002.

[55] P.R. Sivashankari, M. Prabaharan, Three-dimensional porous scaffolds based on agarose / chitosan / graphene oxide composite for tissue engineering, Int. J. Biol. Macromol. 146 (2020) 222–231. https://doi.org/10.1016/j.ijbiomac.2019.12.219.

[56] H.J. Lee, S.H. Ahn, G.H. Kim, Three-dimensional collagen/alginate hybrid scaffolds functionalized with a drug delivery system (DDS) for bone tissue regeneration, Chemistry of Materials. 24 (2012) 881–891. https://doi.org/10.1021/cm200733s.

[57] J. Elango, J. Zhang, B. Bao, K. Palaniyandi, S. Wang, W. Wu, J.S. Robinson, Rheological, biocompatibility and osteogenesis assessment of fish collagen scaffold for bone tissue engineering, Int. J. Biol. Macromol. 91 (2016) 51–59. https://doi.org/10.1016/j.ijbiomac.2016.05.067.

[58] R. Pallela, J. Venkatesan, V.R. Janapala, S.K. Kim, Biophysicochemical evaluation of chitosan-hydroxyapatite-marine sponge collagen composite for bone tissue engineering, Journal of Biomedical Materials Research A. 100A (2012) 486–495. https://doi.org/10.1002/jbm.a.33292.

[59] H. Xie, X. Chen, X. Shen, Y. He, W. Chen, Q. Luo, W. Ge, W. Yuan, X. Tang, D. Hou, D. Jiang, Q. Wang, Y. Liu, Q. Liu, K. Li, Preparation of chitosan-collagen-alginate composite dressing and its promoting effects on wound healing, Int. J. Biol. Macromol. 107 (2018) 93–104. https://doi.org/10.1016/j.ijbiomac.2017.08.142.

[60] A. Susanto, S. Susanah, B.P. Priosoeryanto, M.H. Satari, I. Komara, The effect of the chitosan-collagen membrane on wound healing process in rat mandibular defect, J. Indian. Soc. Periodontol. 23 (2019) 113–118. https://doi.org/10.4103/jisp.jisp_232_18.

[61] A.T. Shah, S. Zahid, F. Ikram, M. Maqbool, A.A. Chaudhry, M.I. Rahim, F. Schmidt, O. Goerke, A.S. Khan, I. ur Rehman, 2019. Tri-layered functionally graded membrane for potential application in periodontal regeneration. Materials Science and Engineering C. 103, 109812. https://doi.org/10.1016/j.msec.2019.109812.

[62] A. Mocan, A. Diuzheva, S. Bădărău, C. Moldovan, V. Andruch, S. Carradori, C. Campestre, A. Tartaglia, M. Simone, D. Vodnar, M. Tiecco, R. Germani, G. Crişan, M. Locatelli, 2019. Liquid phase and microwave-assisted extractions for multicomponent phenolic pattern determination of five Romanian Galium species coupled with bioassays. Molecules. 24, 1226. https://doi.org/10.3390/molecules24071226.

[63] X. Han, Y. Mi, Y. Ji, M. Sun, H. Tang, F. Dong, Z. Guo, 2024. A novel chitosan antioxidant bearing sulfhydryl group: Synthesis, characterization and activity assessment. Int. J. Biol. Macromol. 261, 129816. https://doi.org/10.1016/j.ijbiomac.2024.129816.

[64] W. Tan, J. Zhang, X. Zhao, F. Dong, Q. Li, Z. Guo, Synthesis and antioxidant action of chitosan derivatives with amino-containing groups via azide-alkyne click reaction and N-methylation, Carbohydr. Polym. 199 (2018) 583–592. https://doi.org/10.1016/j.carbpol.2018.07.056.

[65] S. Rindhe, M. Rode, B. Karale, 2010. New benzofuran derivatives as an antioxidant agent, Indian J. Pharm. Sci. 72, 231. https://doi.org/10.4103/0250-474X.65022.

[66] J. Cho, C. Park, Y. Lee, S. Kim, S. Bose, M. Choi, A.S. Kumar, J.-K. Jung, H. Lee, Neuroprotective and Antioxidant Effects of Novel Benzofuran-2-Carboxamide Derivatives, Biomol. Ther. (Seoul). 23 (2015) 275–282. https://doi.org/10.4062/biomolther.2015.030.

[67] T. Zheng, P. Tang, G. Li, 2023. Development of composite film based on collagen and phenolic acid-grafted chitosan for food packaging. Int. J. Biol. Macromol. 241, 124494. https://doi.org/10.1016/j.ijbiomac.2023.124494.

[68] A.C.L. Campos, A. Borges-Branco, A.K. Groth, Wound healing, ABCD. Arquivos Brasileiros de Cirurgia Digestiva. 20 (2007) 51–58. https://doi.org/10.1590/S0102-67202007000100010.

[69] C.A. Balbino, L.M. Pereira, R. Curi, Mechanisms involved in wound healing: a revision, Brazilian Journal of Pharmaceutical Sciences. 41 (2005) 27–51. https://doi.org/10.1590/s1516-93322005000100004.

907 [70] International Organization for Standardization, Biological evaluation of
908 medical devices. Part 5: tests for in vitro cytotoxicity, 3rd ed., ISO 10993-5
909 Switzerland, 2009.

910 [71] N. Thitilertdecha, P. Chaiwut, N. Saewan, 2020. In vitro antioxidant
911 potential of Nephelium lappaceum L. rind extracts and geraniin on human
912 epidermal keratinocytes. Biocatal. Agric. Biotechnol. 23, 101482.
913 https://doi.org/10.1016/j.bcab.2019.101482.

914 [72] F. Blažević, T. Milekić, M.D. Romić, M. Juretić, I. Pepić, J. Filipović-Grčić,
915 J. Lovrić, A. Hafner, Nanoparticle-mediated interplay of chitosan and melatonin
916 for improved wound epithelialisation, Carbohydr. Polym. 146 (2016) 445–454.
917 https://doi.org/10.1016/j.carbpol.2016.03.074.

918 [73] V. Patrulea, V. Ostafe, G. Borchard, O. Jordan, Chitosan as a starting
919 material for wound healing applications, European Journal of Pharmaceutics and
920 Biopharmaceutics. 97 (2015) 417–426.
921 https://doi.org/10.1016/j.ejpb.2015.08.004.

922 [74] R. Guo, S. Xu, L. Ma, A. Huang, C. Gao, The healing of full-thickness burns
923 treated by using plasmid DNA encoding VEGF-165 activated collagen-chitosan
924 dermal equivalents, Biomaterials. 32 (2011) 1019–1031.
925 https://doi.org/10.1016/j.biomaterials.2010.08.087.

926